
Gas hydrate distributions in sediments of pockmarks from the Nigerian Margin - Results and interpretation from shallow drilling

Wei Jiangong^{1, *}, Pape Thomas¹, Sultan Nabil², Colliat Jean-Louis³, Himmler Tobias^{1,2}, Ruffine Livio², De Prunelé Alexis², Dennielou Bernard², Garziglia Sebastien², Marsset Tania², Peters Carl A.^{1,5}, Rabiul Abdulkarim⁴, Bohrmann Gerhard¹

¹ MARUM, University of Bremen, Klagenfurter Str., 28359 Bremen, Germany

² IFREMER, Département REM, Unité des Géosciences Marines, F- 29280 Plouzané, France

³ Total, Pau, av. Larribau, France

⁴ Nigeria Institute for Oceanography and Marine Research, Nigeria

⁵ Department of Earth and Planetary Sciences, Macquarie University, Sydney, NSW 2109, Australia

* Corresponding author : tel.: +49(0)421 218 65055 ; email addresses : jwei@marum.de ; yourbabyface2010@hotmail.com

Abstract :

A joint research expedition between the French IFREMER and the German MARUM was conducted in 2011 using the R/V Pourquoi pas? to study gas hydrate distributions in a pockmark field (1141 – 1199 meters below sea surface) at the continental margin of Nigeria. The sea floor drill rig MeBo of MARUM was used to recover sediments as deep as 56.74 meters below seafloor. The presence of gas hydrates in specific core sections was deduced from temperature anomalies recorded during continuous records of infrared thermal scanning and anomalies in pore water chloride concentrations. In situ sediment temperature measurements showed elevated geothermal gradients of up to 258 °C/km in the center of the so-called pockmark A which is up to 4.6 times higher than that in the background sediment (72 °C/km). The gas hydrate distribution and thermal regime in the pockmark are largely controlled by the intensity, periodicity and direction of fluid flow. The joint interaction between fluid flow, gas hydrate formation and dissolution, and the thermal regime governs pockmark formation and evolution on the Nigerian continental margin.

Keywords : gas hydrate, pockmark, chloride profile, infrared thermal imaging, fluid flow, Nigerian continental margin, MeBo drill rig

40 1. Introduction

41 Pockmarks are circular to elongated seafloor depressions which are often associated with
42 fluid flow from the subsurface (Judd and Hovland, 2007). Submarine pockmarks with
43 various sizes, shapes and state of activity have been widely discovered at different water
44 depths (e.g. Bünz et al., 2003; Chen et al., 2010; Dondurur et al., 2011; Pilcher and
45 Argent, 2007; Pinet et al., 2010; Sahling et al., 2008; Sun et al., 2011; Ussler et al., 2003).
46 In addition, buried paleo-pockmarks found during seismic investigations were proposed
47 to be associated with periodic fluid flow activity in the past (Andresen et al., 2008).

48 Depending on the local geological conditions, several mechanisms have been suggested
49 to explain the process of pockmark formation. Researchers tend to agree that pockmarks
50 are directly or indirectly caused by upward fluid flow from the deep subsurface, through
51 moderate to violent processes (Chand et al., 2012; Gay et al., 2006a; Gay et al., 2006b;
52 Hartwig et al., 2012; Moss et al., 2012; Paull et al., 2008; Riboulot et al., 2013; Rise et al.,
53 1999). In particular on continental margins, methane oversaturated in upward migrating
54 fluids reacts under high pressure and low temperature in shallow sediment to form solid
55 gas hydrate (Matsumoto et al., 2011; Sloan and Koh, 2007). The structural properties of
56 gas hydrate, like its fabric, and the hydrate saturations in the sediment, are largely
57 controlled by the intensity and distribution of fluid flow and by the sediment properties,
58 including permeability and strength (Abegg et al., 2007). Moreover, fluid migration
59 patterns are changed by pore space blocking caused by gas hydrate formation (Bangs et
60 al., 2011; Riedel et al., 2006). The interaction between fluid flow, gas hydrates and host
61 sediment increases the complexity of the pockmark system and is of significant

62 importance when studying the formation and evolution of deep-water pockmark located
63 in the gas hydrate stability zone (GHSZ).

64 Sultan et al. (2010) proposed an initial model for the formation of individual pockmarks
65 on the Nigerian continental margin. Based on gas hydrate findings in shallow sediments
66 and numerical modeling of the dynamic response of the gas hydrate to changes in gas
67 concentrations underneath the gas hydrate occurrence zone (GHOZ), gas hydrate
68 formation and dissolution was suggested to be the major control for the evolution of these
69 pockmarks. In order to gain further insight, a joint research expedition (Guineco-MeBo)
70 between the French IFREMER and the German MARUM with the R/V *Pourquoi pas?*
71 and the portable sea floor drill-rig MeBo was conducted in 2011. The major objective of
72 the expedition was to reveal gas hydrate distributions in even deeper sediments, which
73 eluded sampling with common sampling techniques (e.g., long piston cores) before.

74 In this study, gas hydrate distributions in sediments of selected pockmarks were
75 determined using infrared (IR) thermal scanning of core liners and pore water chloride
76 analysis. Furthermore, the impact of fluid flow and gas hydrate formation/dissolution on
77 controlling the geothermal regime and evolution of the pockmarks is discussed.

78 **2. Geological settings**

79 Our study area is a pockmark field located within the Gulf of Guinea on the continental
80 margin offshore Nigeria (Fig. 1). This continental margin is undergoing slow deformation
81 by gravity tectonism that initiated in response to both, rapid seaward progradation and
82 loading huge amount of sediment (Damuth, 1994). Damuth (1994) distinguished this area

83 into three subareas based on the structural styles: 1) an upper extensional zone, 2) an
84 intermediate translational zone, and 3) a lower compressional zone. The pockmark field
85 studied in this paper is located in the translational zone which is characterized by diapirs
86 underneath. Examples of seismic recordings of shale diapirs in this area can be found in
87 Damuth (1994) and Cohen and McClay (1996).

88 The Nigerian continental margin is an active fluid flux area as indicated from various
89 seafloor features, such as pockmarks, mud volcanoes, gas hydrates and carbonate
90 concretions (Bayon et al., 2007; Brooks et al., 2000; Graue, 2000; Hovland et al., 1997).
91 Formation of such authigenic carbonates is typically attributed to the anaerobic methane
92 oxidation (AOM; Ritger 1987). Pronounced bottom simulating reflectors (BSR),
93 demonstrating the boundary between the base of the GHSZ and free gas underneath, were
94 reported (Cunningham and Lindholm, 2000). Such BSRs indicate the presence of gas
95 hydrates related to high methane flux towards shallow sediments caused by fluid
96 migration (Hovland et al., 1997). In addition, gas chimneys found in the subsurface were
97 proposed to serve as pathways for fast hydrocarbon migration between reservoirs and the
98 seafloor (Heggland, 2003).

99 The pockmark field, comprising the pockmarks A and C studied herein, lies at water
100 depths between 1141 and 1199 m. Pockmark A (Fig. 1C) is a slightly NE-SW elongated
101 seafloor feature with a hummocky topography in the center. The hummocky area
102 corresponds to high multibeam backscatter (George and Cauquil, 2007) which may
103 indicate the occurrence of shallow gas hydrates, free gas and/or authigenic carbonates
104 (Carson et al., 1994). Pockmark C (Fig. 1D) is a pockmark cluster composed of at least

105 three pockmarks (C1 – C3). Shallow gas hydrates were found widely in this pockmark
106 field which might contribute to the formation of the pockmarks (Sultan et al., 2010).
107 Authigenic carbonates were also recovered from different depths in these pockmarks
108 (Sultan et al., 2010).

109 **3. Material and methods**

110 **3.1 MeBo drilling**

111 The mobile drilling system MeBo (Freudenthal and Wefer, 2013) was deployed from the
112 R/V ‘*Pourquoi pas?*’ to drill 12 cores of up to 56.74 m in length in the pockmark field
113 between 1141 and 1199 m water depth (Fig. 1; Table 1). Seven drill sites were located in
114 and around pockmark A (Fig. 1C), with five sites in the central part (GMMB06, 07, 08,
115 10 and 11) and two in the periphery (GMMB03 and 12). Two drill sites (GMMB01 and
116 02) were located outside (NW) pockmark A. Further three drill sites (Fig. 1D) were
117 located in pockmark C1 (GMMB04), pockmark C2 (GMMB05), and SE of pockmark C2
118 (GMMB09), respectively.

119 **3.2 Infrared thermal imaging of MeBo cores**

120 Infrared (IR) temperature profiles of the 2.52 m-long MeBo core liners were obtained for
121 10 drill sites in order to document the gas hydrate distribution in the MeBo cores. Images
122 for GMMB10 were not interpreted due to their low quality. The core liners were removed
123 from the core barrels immediately after recovery on deck. After a quick cleaning of the
124 liner surfaces, pictures were taken with an IR camera (ThermaCam SC 640 camera, FLIR
125 Systems) for documenting temperature variations. The temperature measurements of the

126 IR system ranged from $-40\text{ }^{\circ}\text{C}$ to $+120\text{ }^{\circ}\text{C}$ and the precision of the camera was $0.1\text{ }^{\circ}\text{C}$ at
127 $30\text{ }^{\circ}\text{C}$ with the accuracy of $\pm 2\text{ }^{\circ}\text{C}$. Each thermal scan covered approximately 60 cm depth
128 range of the core. Five to six pictures including a spatial overlap of about 10 cm were
129 taken from each liner in less than one minute.

130 For an individual drilling station, all IR images were combined in one figure to display
131 the temperature distribution for the entire core surface. The raw data were converted and
132 exported as bitmap format using the ThermaCAM™ Researcher Professional software.
133 The bitmap files were processed using commercially available graphical software. All IR
134 images were merged consecutively, considering distinct hot or cold spots as reference
135 points. Temperatures along the central axis of the cores were extracted from the IR
136 images to obtain temperature logs (Fig. 2). Surface temperatures of core liners containing
137 sediment devoid of gas hydrates were considered as background temperature. At each
138 drilling station, background temperatures varied slightly (ca. $1\text{--}2\text{ }^{\circ}\text{C}$) between individual
139 liners due to different *in situ* sediment temperatures and/or slightly different times
140 required for individual liner handling (equilibration with ambient temperature of $\approx 30\text{ }^{\circ}\text{C}$
141 on ship's deck). Thus, the specific background temperature was assigned to each core
142 liner individually.

143 The difference between liner surface temperature and background temperature (ΔT) was
144 calculated to interpret the content of the cores. In order to obtain a better visualization
145 and to minimize the artifacts for further analysis, only anomalies with $\Delta T > +1\text{ }^{\circ}\text{C}$ were
146 considered as voids in the liner and $\Delta T < -2\text{ }^{\circ}\text{C}$ were considered to represent hydrate-
147 bearing sediment, as hydrate dissociation is an endothermic process.

148 **3.3 Pore water chloride and sulfate analysis**

149 Pore water was extracted using Rhizon samplers (Seeberg-Elverfeldt et al., 2005), which
150 consists of a thin tube made up with hydrophilic porous polymer with pore diameters of
151 approximate 0.2 μm . The Rhizon samplers were pushed into the sediment through holes
152 drilled through the plastic liners. 10 or 20 ml plastic syringes were connected to the
153 sampler to create a vacuum and collect the pore water. Extracted pore water was split,
154 prepared for various analyses, and stored in the refrigerator or reefer. Sulfate and chloride
155 concentrations were measured on-board by using ion chromatography (861 Advanced
156 Compact IC, 837 IC Eluent Degasser, and Advanced Sample Processor by Metrohm).

157 For several MeBo stations, seawater-derived sulfate in detectable concentrations was not
158 only found in near-surface sediments but also in deeper layers. This was unexpected
159 because sulfate is typically depleted below the sulfate-methane interface (SMI) due to
160 AOM. Moreover, since measured sulfate concentrations below the SMI scattered
161 considerably, we assumed that the presence of sulfate in these core sections were artifacts
162 caused during the core drilling/handling procedure. Therefore, concentrations of chloride
163 were re-calculated assuming the absence of sulfate below the SMI. This procedure caused
164 changes in absolute chloride concentrations of <20% but affected trends in chloride
165 profiles insignificantly.

166 **3.4 In situ temperature measurements**

167 In-situ temperature measurements were conducted in pockmark A using autonomous
168 miniaturized temperature loggers (MTLs) from ANTARES Datensystem GmbH

169 (Germany), which have already been used successfully during previous studies (Römer et
170 al., 2012; Feseker et al., 2009; Pape et al., 2011). Five temperature sensors were mounted
171 on outriggers attached to the cutting barrel of a 6 m-long gravity corer according to
172 Feseker et al. (2009). Distances between the loggers were 100 cm and the logging time
173 interval was set to 5 sec. For each deployment, the gravity corer was held 50 meters
174 above the seafloor for three to four minutes to measure the water temperature for
175 calibration purposes of each MTL. Based on these measurements the standard deviation
176 of the five loggers was calculated to be smaller than 0.008 °C (Table 2). At each station,
177 the loggers were left in the sediment for about 15 minutes (Fig. 5) after penetration of the
178 gravity corer to adjust to the sediment temperature. The absolute penetration depths could
179 be estimated from mud smear on the gravity corers or on the cable. By using linear
180 regression individual temperatures recorded with the MTLs and assumed penetration
181 depths were used to calculate the site-specific geothermal gradients.

182 **4. Results**

183 MeBo was deployed 12 times in total during the entire cruise. Depending on the lithology
184 as well as on gas and gas hydrate contents, the recovery of the drill cores ranged between
185 60% and 94% with a mean of 81%. The cores comprised homogenous hemipelagic dark
186 greyish clay with sporadic authigenic carbonate concretions. Distinct depth-changes or
187 lateral variations of sediment grain sizes were not observed. Sediments with elevated
188 water content, which was attributed to ex situ gas hydrate dissociation, were observed at
189 different depths without regularity. No relation between gas hydrate distributions and
190 sediment grain sizes became obvious.

191 **4.1 Infrared thermal imaging**

192 Infrared (IR) temperature profiles of core liners were established for most of the drill sites.
193 The only exceptions were station GMMB01 and GMMB02 outside of pockmark A since
194 indications for the presence of gas hydrates in sediments within the penetration depth
195 (53.3 meters below seafloor (mbsf)) at these drill sites were missing in seismic profiles
196 (Sultan et al., 2010). The assumption of the gas hydrates absence in these sediments was
197 confirmed by the subsequent pore water chloride profiling (see chapter 4.2).

198 Comparison of IR images with lithological core descriptions and high-resolution core
199 photographs showed that thermal regimes of the MeBo cores were mainly determined by
200 the core contents. This is exemplary shown for core GMMB06 (Fig. 2). Since the *in situ*
201 temperature of sediment (~4.5 °C) was significantly lower than that of the upper water
202 column (up to ~28 °C) and the atmosphere (~30 °C), the cores were continuously warmed
203 up during the core recovery and handling on deck. Liners filled with sediment exhibited
204 intermediate temperatures of 23–25 °C (Fig. 2A), depending mainly on the duration they
205 were exposed to the water column and air before being imaged. These temperatures were
206 considered as background.

207 Cores containing dissociating gas hydrates yielded prominent cold anomalies since
208 hydrate dissociation happening during core recovery and handling is an endothermic
209 process. The temperature decrease is mainly influenced by the volume of gas hydrate
210 pieces and the decomposition speed. The extent of cold temperature zones reflects in
211 many ways the fabric of gas hydrates in the liners. Disseminated gas hydrates are prone
212 to dissociation in a relatively short time. After a very short time of dissociation-induced

213 cooling which occurs relatively homogenously throughout a respective core section
214 temperature re-increases. Because of the relatively small amount of water released during
215 decomposition of disseminated hydrates, residual sediments often show a moussy fabric
216 (Weinberger et al., 2005) and exhibit moderate negative ΔT of $-3\text{ }^{\circ}\text{C}$ to $-4\text{ }^{\circ}\text{C}$ (Fig. 2B).
217 In contrast, nodular gas hydrates, massive hydrate layers or hydrate-filled fractures
218 usually occurring in distinct intervals reveal stronger negative ΔT of up to $-10\text{ }^{\circ}\text{C}$ (Fig.
219 2C). Decomposition of such hydrate fabrics principally takes much longer time than that
220 of disseminated hydrates because of both, their comparably smaller surface area and the
221 resulting higher efficiency of the self-preservation effect (Sloan and Koh, 2007). During
222 decomposition of nodular/massive hydrates the residual sediment might become very
223 soupy because of the high volume of hydrate water released.

224 Voids or gaps defined as empty intervals in the liners are often due to gas expansion.
225 They are typically represented by positive ΔT of $+2\text{ }^{\circ}\text{C}$ to $+4\text{ }^{\circ}\text{C}$ (Fig. 2A and 2C)
226 because the effective heat capacity of the gas/air filled liner strongly differs from that of
227 sediments and the temperature gets into equilibrium with the ambient air rapidly. Voids
228 within gas hydrate-bearing sediments (Fig. 2C) are generated by gas expansion likely
229 caused by gas release from hydrate dissociation. In contrast, voids within non-hydrate
230 sediment (Fig. 2A), are likely caused by methane release from the dissolved phase due to
231 the pressure drop during core recovery. High-temperature patches with absolute
232 temperatures of more than $30\text{ }^{\circ}\text{C}$ as shown in Fig. 2A are core handling artifacts.

233 Since the IR thermal patterns of the cores are mainly controlled by their contents, they
234 were classified into four groups (Fig. 3).

235 IR-temperature pattern 1: Sediment without gas hydrates

236 Homogenous hemipelagic sediment was represented by moderate temperatures of 23–
237 25 °C (Fig. 2A). It was present in the top few meters of all cores (from 1.2 mbsf in
238 GMMB11 to 38.5 mbsf in GMMB09). It also occurred at the bottom of some cores below
239 the gas hydrate occurrence zone (GHOZ), including GMMB03, GMMB05, GMMB08
240 and GMMB12 (Fig. 3).

241 IR-temperature pattern 2: Sediment with gas hydrate

242 Gas hydrate-bearing sediments showed relatively low temperatures (less than ~22 °C) of
243 the liner surface (Fig. 2B and 2C). Associated voids represented by positive ΔT were also
244 observed. Since the voids are mainly caused by gas expansion during hydrate dissociation,
245 which pushes the sediments apart, void intervals were included in pattern 2 as well.

246 IR-temperature pattern 3: High gas concentration

247 This temperature pattern was defined for core sections with relative moderate temperature
248 between 23 and 25 °C, separated by distinct voids represented by slightly warmer
249 temperatures of ~27 °C. In some gas hydrate-free sediment intervals, cm-scaled voids
250 appeared in a dense pattern and revealed positive ΔT in the IR images (e.g. 30.0-38.5
251 mbsf in core GMMB09; Fig. 3). Formation of voids is attributed to the expansion of
252 methane gas excluded from the dissolved phase due to depressurization.

253 IR-temperature pattern 4: Intervals of unidentified liner content

254 Large unfilled sections adjacent to gas hydrate-bearing sediment were occasionally
255 observed, for example in GMMB07 and GMMB11 (Fig. 3). However, it remained
256 unclear whether gas hydrates were present in these sections prior to IR imaging. Thus, we
257 defined these core sections as intervals of unidentified liner content.

258 **4.2 Pore water chloride concentrations**

259 Chloride concentrations in pore waters of 12 MeBo cores were measured to study vertical
260 gas hydrate distributions and to compare the results with those obtained by IR thermal
261 scanning (Fig. 3). Chloride concentrations in bottom waters were around 550 mM and
262 were also measured in near-surface sediments. With increasing depth, Cl⁻ concentrations
263 showed a slightly decreasing trend in some cores such as GMMB08 and GMMB03. By
264 considering Cl⁻ = 550 mM as background, discrete positive and negative
265 concentration anomalies were identified in the cores. Negative anomalies, with minimum
266 concentrations of 213.1 mM at 38.83 mbsf in core GMMB09, were found widely
267 distributed in gas hydrate-bearing sediments. These were caused by the dilution of pore
268 water by Cl⁻-free water which is released by hydrate dissociation during core recovery
269 (Torres et al., 2004a; Tréhu et al., 2004). Discrete positive Cl⁻ anomalies, of up to 1059.7
270 mM, in contrast are proposed to be associated with fast hydrate formation. During
271 formation of gas hydrates ions are excluded from the hydrate lattice, which results in an
272 increases in pore water chloride concentrations (Torres et al., 2011; Torres et al., 2004b).
273 In previous studies it was observed that for chloride back diffusion to background
274 concentrations takes a comparably long time (Haeckel et al., 2004). Therefore, positive
275 anomalies existing *in situ* can still be detected by conventional pore water analysis in case

276 quick sampling prevents pore water dilution by fresh water from dissociating hydrates.
277 Since the pore water samples were taken immediately before the massive hydrates were
278 totally decomposed, the elevated chloride concentrations are a proxy for relatively recent
279 hydrate formation in sediments of the pockmarks.

280 **4.3 Regional and depth variations in gas hydrate distributions**

281 Both proxies, IR imaging and pore water chloride concentration profiling, revealed
282 similar gas hydrate down core distributions and only for some small intervals results from
283 both methods did not correlate (Table 1). Hydrates in pockmark A were present in the
284 central part at much shallower depth compared to the periphery (Fig. 3, Table 1).
285 Temperature anomalies captured by the IR images indicated that the top of the GHZO in
286 the central part (GMMB06, GMMB07, GMMB08 and GMMB11) ranges from 2.3 mbsf
287 (GMMB08) to 6.5 mbsf (GMMB11), whereas chloride anomalies revealed hydrate
288 presence from 1.2 mbsf (GMMB11) to 4.4 mbsf (GMMB10). Peripheral cores
289 (GMMB03 and GMMB12) showed down core gas hydrate presence from 6.9 to 7.6 mbsf
290 by using IR imaging and 6.1 to 6.7 mbsf based on chloride anomalies (Fig. 3). These data
291 sets substantiate a very shallow top of the GHZO in the pockmark center which deepens
292 towards its rim as already suggested by Sultan (2010). In core GMMB08, taken in the
293 NW central part of pockmark A, the down core gas hydrate distribution was indicated by
294 IR imaging down to 26.4 mbsf and by the chloride proxy down to 24.1 mbsf. In cores
295 GMMB03 and GMMB12 taken at the periphery of pockmark A, gas hydrate occurrences
296 were present from about 7 mbsf down to about 17 mbsf.

297 In pockmarks C1 and C2, the top of the GHZOZ was determined to be positioned between
298 5.9 mbsf and 10.3 mbsf using IR imaging proxy, and 5.3 mbsf and 8.5 mbsf using
299 chloride anomalies (Fig. 3). Outside pockmark C2, core GMMB09 showed the deepest
300 gas hydrate occurrence of all MeBo cores from about 38.5 mbsf down to its maximum
301 penetration depth of 43.6 mbsf (Fig. 3).

302 **4.4 In situ sediment temperatures**

303 In situ temperature measurements conducted at ten stations in pockmark A using MTLs
304 showed slight variations in water temperatures ranging between 4.45 and 4.53 °C (Fig. 4,
305 Table 2). For the *in situ* sediment temperature measurements most geothermal gradients
306 showed linear or sub-linear slopes. The thermal gradient established at station GMGCT22,
307 which was performed outside pockmark A and is considered as reference station, was
308 about 72 °C/km. Similar thermal gradients ranging between 51 and 79 °C/km were
309 determined for four other stations (GMGCT23, 24, 41 and 49). At a cluster of five
310 stations performed in the hummocky area elevated geothermal gradients were observed.
311 Slightly elevated gradients of 112 and 119 °C/km were measured at stations GMGCT46
312 and -47, respectively. At stations GMGCT44, -45 and -40, the gradients were 198 and
313 330 °C/km, which is 2.8 and 4.6 times higher than the gradient at the background station,
314 respectively. At station GMGCT40 a considerably elevated temperature deviating from
315 the general trend established by the other MTLs was measured with TL-2 at a sediment
316 depth of about 2 mbsf (Fig. 4).

317 **5. Discussion**

318 **5.1 Thermal regime of pockmark A**

319 The geothermal gradient in the central part of pockmark A was significantly higher than
320 the local background gradient (Fig. 4). Elevated temperatures in marine sediments caused
321 by fluid flow have been widely reported from active mud volcanoes (e.g. Feseker et al.,
322 2008; 2009a;b; Foucher et al., 2010) and other marine seep types (Römer et al., 2012). At
323 pockmark A studied herein indications for mud flow activities such as mud breccia (Kopf,
324 2002) have not been found. However, free gas ebullition observed above the central part
325 of pockmark A during the expedition (for location see Sultan et al., 2014) proves fluid
326 upward migration at this structure. Thus, the temperature elevation in shallow sediment is
327 likely caused by fluid advection.

328 It is worth noting that none of our measured geothermal profiles is strictly linear. We
329 assume that besides the influence from heat convection induced by fluid flow,
330 precipitation of gas hydrates in pore space contributes partially to this phenomenon.
331 Several physical bulk sediment properties (i.e. thermal conductivity, heat capacity,
332 density) are altered by gas hydrate precipitation in the pore space. In particular, gas
333 hydrate formation is an exothermic reaction and heat is released when hydrate crystallizes
334 (Sloan and Koh, 2007; Waite et al., 2007). Waite et al. (2007) pointed out that the thermal
335 diffusivity of sediment with 60% porosity and 40% gas hydrate saturation increases by
336 20% compared to that of non-hydrate-bearing sediment. The gas hydrate saturation in the
337 studied pockmarks is not quantified yet. Nevertheless, we conservatively estimate that
338 gas hydrate saturations in specific sediment depths do not exceed 40% and that deviations

339 of absolute temperatures caused by hydrates are <20% with respect to a hypothetical
340 linear thermal gradient throughout the sediment.

341 At station GMGCT40 (Fig. 4) an exceptionally high temperature was measured with TL-
342 2 if compared to the other temperature loggers mounted below and above. This
343 phenomenon was also observed at a high-flux seep area in the Black Sea (Römer et al.,
344 2012). Fig. 5 shows the continuous temperature change with time recorded with the
345 loggers during stations GMGCT40 and 41 when the corer has not been lifted out of the
346 water. It becomes obvious that at station GMGCT40 the absolute temperature measured
347 with TL-2 was generally highest and that the temperature slope reversed after a while.
348 Temperatures determined with TL-1, -3, and -4 were lower and reached equilibrium in
349 contrast to that of TL-2. During station GMGCT41 absolute temperatures changed
350 according to the expected order which corresponded to the arrangement of loggers at the
351 gravity corer.

352 The temperature difference between TL-1 and TL-2 is 0.127 °C which is two orders of
353 magnitude higher than the logger accuracy (see Table 2). Thus, we conclude that the
354 temperature measured with TL-2 was neither noise nor caused by wrong operation.
355 However, if we ignore the temperature measured with TL-2, temperatures determined
356 with the other three loggers show a linear regression with a slope similar to those of
357 GMGCT44 (198°C/km) and GMGCT45 (258°C/km) (see Fig. 4).

358 The exceptionally high temperature recorded at about 2 mbsf at station GMGCT40 can
359 not be explained by vertical fluid advection and/or sediment thermal properties changed
360 by hydrate formation. It is obvious that additional heat was generated at the depth

361 between TL-1 and TL-3. In a 3D complex pockmark, spatially restricted temperature
362 elevations might be caused by lateral heat advection from fluid flow along fractures or
363 fast gas hydrate formation. Gas hydrate formation and dissociation are exothermic and
364 endothermic processes, respectively, which subsequently change the thermal regime of
365 pockmarks (Chen and Cathles, 2005). During the cruise, gas hydrate with bubble fabric,
366 which is an indication of fast gas hydrate crystallization from methane bubbles
367 (Bohrmann et al., 1998), was sampled with gravity cores. Since gas hydrate occurs
368 widely in the center of pockmark A, its crystallization could release significant amounts
369 of heat (Chen and Cathles, 2005). Although we did not further investigate the amount of
370 freshly formed hydrate required to induce the relative temperature increase observed, we
371 speculate that TL-2 might have intersected with a fracture in which either gas hydrate
372 precipitated rapidly and/or fluid flowed happened facilitating lateral heat convection.

373 Because gas hydrates are sensitive to temperature variations (e.g. Feseker et al., 2009b;
374 Pape et al., 2011; Römer et al., 2012; Berndt et al., 2014) thermal variations in the
375 sediment impact gas hydrate distributions. At active seeps, temperature elevation in
376 shallow sediments due to fluid advection lift the base of the GHSZ (e.g. Ginsburg et al.,
377 1999; Römer et al., 2012). Considering the maximum (258 °C/km) and minimum
378 (72 °C/km) geothermal gradients determined in this study (Table 2), the base of the
379 GHSZ under pockmark A should be situated between 35 mbsf and 130 mbsf, respectively
380 (Fig. 6). Since high thermal gradients were detected only in a restricted area NW of the
381 geometrical center of the pockmark, we assume that distinct temperature elevations
382 caused by fluid advection influence the GHSZ only on a small scale. In the water column,

383 the top of the GHSZ is estimated to be at 587 mbsl which is consistent with the maximum
384 height of gas flares observed above pockmark A during the cruise (Sultan et al., 2014).

385 **5.2 Gas hydrate and fluid flow**

386 Results from IR scanning and pore water chloride concentration analysis of the MeBo
387 cores as well as recoveries substantiate gas hydrate presence in shallow (meters to tens of
388 meters depth) sediments of the three studied pockmarks. It was shown that shallow gas
389 hydrates at active marine seeps primarily form from free gas (Haeckel et al., 2004; Römer
390 et al., 2012; Sahling et al., 2008; Torres et al., 2004b; Wallmann et al., 2006). Gas flares
391 observed above pockmark A during the survey in 2011 are direct evidence of gas flow
392 through the sediment (Sultan et al., 2014). Therefore, we assume that gas hydrates in the
393 studied pockmarks are mainly formed from the free gas phase. Free gas captured in
394 pockets within the GHOZ might contribute to the high amplitude reflectors observed in
395 seismic records from that area (Figs .7). In particular, at station GMMB04 in pockmark
396 C1 showed vigorous gas expulsion during drilling at ~18 mbsf, which corresponds to
397 distinct high amplitude reflectors (Fig. 7B) (Sultan et al., 2014).

398 Free gas can migrate along fractures and gas hydrate can precipitate along fracture walls
399 (Torres et al., 2004b; Flemings et al., 2003) where fluid pressure and crystallization
400 forces are less than the effective overburden stress. In case free methane-rich gas
401 migrates upward into shallow sediment, where fluid pressure and crystallization force
402 exceed the effective overburden stress, it spreads out in the pore space and reacts with
403 water, forming gas hydrate (Torres et al., 2004b). This assumption is supported by our
404 observation of gas hydrates present within the upper ~30m (Figs. 2, 3, 7). Because the

405 maximum depth of the GHSZ at pockmark A is situated at around 130 mbsf (geothermal
406 gradient: 72 °C/km; Table 2; Fig. 6), we might assume that gas hydrate also forms at
407 greater depth.

408 However, gas flow in a seep system is not under steady state (Bangs et al., 2011; Chand
409 et al., 2012; Gay et al., 2006b; Greinert et al., 2006) and pressure drop in deep gas
410 reservoirs (Bangs et al., 2011) and/or sealing of pathways by gas hydrate formation
411 (Riedel et al., 2006) might result in a decrease, or even cease of gas flow. Thus, although
412 no gas flares were recognized at pockmark C1 and C2 during this expedition, gas
413 hydrates in these two pockmarks likely formed from active gas flow in the recent past.

414 Upward gas migration stimulates the anaerobic methane oxidation (AOM) mediated by
415 methanotrophic archaea and sulfate reducing bacteria in near-surface sediments (Hoehler
416 et al., 1994; Boetius et al., 2000), and the resulting end products, such as hydrogen sulfide,
417 nourish a chemosynthesis-based ecosystem (Sahling et al., 2008). During our expedition
418 living vesicomyid clams, which rely on sulfide oxidation, were recovered from the
419 seafloor in the studied area, indicating a living chemosynthetic ecosystem. However, as
420 mentioned above, gas flow at a seep system is a transient process. Bangs et al. (2011)
421 pointed out that methane gas flow for a vent at Southern Hydrate Ridge has undergone
422 significant reduction or complete interruption within just a few years, whereas the
423 associated ecosystem has persisted for thousands of years. This observation raises the
424 question, how the chemosynthesis-based species survive during periods of reduced gas
425 flow. In a gas hydrate setting methane diffuses continuously from the shallow gas hydrate
426 reservoir towards the methane-depleted sea water and sustains AOM. This is consistent

427 with the assumption of Sultan et al. (2010) that many gas hydrate reservoirs in the study
428 area are currently undergoing dissolution due to insufficient methane supply from greater
429 depth. Similar conclusions of chemosynthetic-based macrofauna presumably relying on
430 continuous methane supply from decomposing hydrates were already proposed for seep
431 systems in other regions (e.g., Paull et al., 1995; Pape et al., 2014). Thus, we propose that
432 gas hydrate reservoirs in shallow sediments serve as a capacitor (see e.g. Dickens, 2003),
433 as they form rapidly during a high gas-flow phase, and sustain the seep ecosystem by
434 slow methane diffusion when the gas flow from below is reduced.

435 **5.3 Pockmark formation**

436 It was initially proposed by Sultan et al. (2010) that gas hydrate dissolution caused by
437 insufficient gas supply is the controlling factor for pockmark formation and evolution in
438 the study area. New field data suggested that pockmark formation is not only controlled
439 by slow gas hydrate dissolution but also by rapid hydrate formation (Sultan et al., 2014).
440 Based on the data obtained from the MeBo cores in this study, an improved but simple
441 model comprising five stages is suggested for the evolution of the pockmarks (Fig. 8) in
442 the studied area

443 Stage A: Gas migrates from a deep source. Within the GHSZ, when the hydrate
444 crystallization force overcomes the burden of the overlying sediment, gas hydrate starts
445 precipitating in the shallow sediment. Gas hydrate growth decreases the pore space
446 availability and sediment permeability and clogs the pathways of fluid flow, which
447 subsequently decreases or even ceases the fluid flow in uppermost sediments. During this

448 stage, there is neither a distinct morphological change on the seafloor nor gas emission
449 into the water column.

450 Stage B: In case of reduced gas flow to shallow sediments, sulfate can penetrate to
451 greater depths, which leads to a downward shift of the SMI (see e.g. Borowski et al.,
452 1996). Methane in the shallow sediment is likely depleted due to diffusion and AOM. As
453 a result, gas hydrates dissolve from the top of the GHOSZ (see Sultan et al., 2010).
454 Subsequently, the overlying sediment is deformed due to the volume loss below and a
455 seafloor depression is created. This stage might explain the ~2 m depression observed for
456 pockmark C2 (Figs. 1 and 7).

457 Stage C: Once the fluid flow is re-intensified, methane and shallow hydrate repeat the
458 same procedure as described in Stage A. When pore pressure surpasses a threshold value,
459 fractures are generated in the overlying sediment at the pockmark center (e.g. observed in
460 pockmark A, Fig. 7) which might serve as pathways for free gas to migrate to the seafloor.
461 Since these fractures form within the GHSZ, gas hydrates might accumulate along the
462 fracture walls which efficiently prevents the contact between pore water and gases. Fast
463 gas hydrate formation will significantly increase the salinity of the surrounding pore
464 water due to ion exclusion and the resulting brine might locally prevent gas hydrate
465 formation (Ussler & Paull, 1995; Torres et al., 2011). Massive gas hydrate accumulating
466 in the shallow sediment expands the mass volume and creates convex-shaped elevations
467 as well as a rough seafloor, like observed close to the center of pockmark A (Fig. 1). This
468 can explain the cones and hummocky structure at the centers of pockmarks A and C1 (Fig.
469 7).

470 Stage D: In case the methane flux is redirected towards shallow sediments in the vicinity
471 of the initial pockmark, a new pockmark might be created and might repeat stages A-C.

472 Stage E: The complexity and size of a pockmark might increase significantly in case
473 more and more new pockmarks morphologically combine (Marcon et al., 2014). It might
474 be assumed that pockmark C1, which exhibits a roughly NE-SW seafloor expression and
475 complex seafloor morphology, is composed of several small pockmarks at different
476 stages.

477 **6. Conclusion**

478 Gas hydrate distributions in the sediment of three pockmarks on the Nigerian continental
479 margin were investigated by applying infrared (IR) thermal imaging and pore water
480 chloride and sulfate concentration measurements on cores recovered with the portable
481 MeBo drill rig. In addition, ten *in situ* sediment temperature measurements were
482 performed to study the geothermal regime of the individual pockmark A. Based on the
483 temperature and chloride anomalies, the following conclusions are drawn:

484 1. Negative temperature anomalies detected by IR thermal scanning as well as positive
485 and negative chloride anomalies in pore waters indicated the presence of gas hydrate in
486 shallow pockmark sediments. Distributions of gas hydrate-bearing sediments as inferred
487 from both methods match each other.

488 2. Geothermal gradients up to 5 times higher in the center of pockmark A than the
489 background were interpreted to result from enhanced heat advection caused in the course
490 of fluid flow and potentially also to fast growth of gas hydrates.

- 491 3. Recent hydrate formation is inferred from positive chloride anomalies.
- 492 4. Gas hydrate precipitation and dissolution caused by the variation of fluid flow exert
493 significant impact on the formation and evolution of pockmarks on the Nigerian
494 continental margin.
- 495

496

497 **Acknowledgement**

498 We thank the captain and crew of *R/V Pourquoi pas?* for support during the Guineco-
499 MeBo cruise in 2011. We thank also the MeBo team from MARUM and the staff of
500 IFREMER for the excellent help during the cruise. We are thankful for the constructive
501 comments from C. Berndt and an anonymous reviewer which helped to improve the
502 manuscript significantly.

503 This work was partly funded through the DFG-Research Center/Excellence Cluster “The
504 Ocean in the Earth System” MARUM – Center for Marine Environmental Sciences. A
505 major financial contribution came from BMBF-project 03G0824A.

506 Data used in the present paper are covered by a confidentiality agreement between Total,
507 IFREMER and MARUM that restrict access; interested readers can contact the authors
508 for more information. J. Wei was sponsored by the China Scholarship Council (CSC).

509

510 **Reference list**

- 511 Abegg, F., Bohrmann, G., Freitag, J., and Kuhs, W., 2007, Fabric of gas hydrate in sediments from Hydrate
512 Ridge—results from ODP Leg 204 samples: *Geo-Marine Letters*, v. 27, no. 2-4, p. 269-277.
- 513 Andresen, K. J., Huuse, M., and Clausen, O. R., 2008, Morphology and distribution of Oligocene and
514 Miocene pockmarks in the Danish North Sea - implications for bottom current: *Basin Research*, v.
515 20, no. 3, p. 445-466.
- 516 Bangs, N. L. B., Hornbach, M. J., and Berndt, C., 2011, The mechanics of intermittent methane venting at
517 South Hydrate Ridge inferred from 4D seismic surveying: *Earth and Planetary Science Letters*, v.
518 310, no. 1–2, p. 105-112.
- 519 Bayon, G., Pierre, C., Etoubleau, J., Voisset, M., Cauquil, E., Marsset, T., Sultan, N., Le Drezen, E., and
520 Fouquet, Y., 2007, Sr/Ca and Mg/Ca ratios in Niger Delta sediments: Implications for authigenic
521 carbonate genesis in cold seep environments: *Marine Geology*, v. 241, no. 1–4, p. 93-109.
- 522 Berndt, C., Feseker, T., Treude, T., Krastel, S., Liebetrau, V., Niemann, H., Bertics, V. J., Dumke, I.,
523 Dünnbier, K., Ferré, B., Graves, C., Gross, F., Hissmann, K., Hühnerbach, V., Krause, S., Lieser,
524 K., Schauer, J., and Steinle, L., 2014, Temporal Constraints on Hydrate-Controlled Methane
525 Seepage off Svalbard: *Science*, v. 343, no. 6168, p. 284-287.
- 526 Boetius, A., Ravensschlag, K., Schubert, C. J., Rickert, D., Widdel, F., Gieseke, A., Amann, R., Jorgensen,
527 B. B., Witte, U., and Pfannkuche, O., 2000, A marine microbial consortium apparently mediating
528 anaerobic oxidation of methane: *Nature*, v. 407, no. 6804, p. 623-626.
- 529 Bohrmann, G., Greinert, J., Suess, E., and Torres, M., 1998, Authigenic carbonates from the Cascadia
530 subduction zone and their relation to gas hydrate stability: *Geology*, v. 26, no. 7, p. 647-650.
- 531 Borowski, W.S., Paull, C.K., Ussler III, W., (1996) Marine pore-water sulfate profiles indicate in situ
532 methane flux from underlying gas hydrate. *Geology*, 24(7), 655-658.

- 533 Brooks, J. M., Bryant, W. R., Bernard, B. B., and Cameron, N. R., 2000, The Nature of Gas Hydrates on
534 the Nigerian Continental Slope: *Annals of the New York Academy of Sciences*, v. 912, no. 1, p.
535 76-93.
- 536 Bünz, S., Mienert, J., and Berndt, C., 2003, Geological controls on the Storegga gas-hydrate system of the
537 mid-Norwegian continental margin: *Earth and Planetary Science Letters*, v. 209, no. 3–4, p. 291-
538 307.
- 539 Carson, B., Seke, E., Paskevich, V., Holmes, M.L., (1994) Fluid expulsion sites on the Cascadia
540 accretionary prism: Mapping diagenetic deposits with processed GLORIA imagery. *J. Geophys.*
541 *Res.*, 99(B6), 11959-11969.
- 542 Chand, S., Thorsnes, T., Rise, L., Brunstad, H., Stoddart, D., Bøe, R., Lågstad, P., and Svolsbru, T., 2012,
543 Multiple episodes of fluid flow in the SW Barents Sea (Loppa High) evidenced by gas flares,
544 pockmarks and gas hydrate accumulation: *Earth and Planetary Science Letters*, v. 331–332, no. 0,
545 p. 305-314.
- 546 Chen, D. F., and Cathles, L. M., 2005, On the thermal impact of gas venting and hydrate crystallization:
547 *Journal of Geophysical Research: Solid Earth*, v. 110, no. B11, p. B11204.
- 548 Chen, S.-C., Hsu, S.-K., Tsai, C.-H., Ku, C.-Y., Yeh, Y.-C., and Wang, Y., 2010, Gas seepage, pockmarks
549 and mud volcanoes in the near shore of SW Taiwan: *Marine Geophysical Researches*, v. 31, no. 1-
550 2, p. 133-147.
- 551 Cohen, H. A., and McClay, K., 1996, Sedimentation and shale tectonics of the northwestern Niger Delta
552 front: *Marine and Petroleum Geology*, v. 13, no. 3, p. 313-328.
- 553 Cunningham, R., and Lindholm, R. M., 2000, *AAPG Memoir 73, Chapter 8: Seismic Evidence for*
554 *Widespread Gas Hydrate Formation, Offshore West Africa.* Damuth, J. E., 1994, Neogene gravity
555 tectonics and depositional processes on the deep Niger Delta continental margin: *Marine and*
556 *Petroleum Geology*, v. 11, no. 3, p. 320-346.

- 557 Dickens, G.R., (2003) Rethinking the global carbon cycle with a large, dynamic and microbially mediated
558 gas hydrate capacitor. *Earth and Planetary Science Letters*, 213(3-4), 169-183.
- 559 Dondurur, D., Çifçi, G., Drahor, M. G., and Coşkun, S., 2011, Acoustic evidence of shallow gas
560 accumulations and active pockmarks in the Izmir Gulf, Aegean sea: *Marine and Petroleum*
561 *Geology*, v. 28, no. 8, p. 1505-1516.
- 562 Feseker, T., Dähmann, A., Foucher, J. P., and Harmegnies, F., 2009a, In-situ sediment temperature
563 measurements and geochemical porewater data suggest highly dynamic fluid flow at Isis mud
564 volcano, eastern Mediterranean Sea: *Marine Geology*, v. 261, no. 1-4, p. 128-137.
- 565 Feseker, T., Foucher, J. P., and Harmegnies, F., 2008, Fluid flow or mud eruptions? Sediment temperature
566 distributions on Håkon Mosby mud volcano, SW Barents Sea slope: *Marine Geology*, v. 247, no.
567 3-4, p. 194-207.
- 568 Feseker, T., Pape, T., Wallmann, K., Klapp, S.A., Schmidt-Schierhorn, F., Bohrmann, G., (2009b) The
569 thermal structure of the Dvurechenskii mud volcano and its implications for gas hydrate stability
570 and eruption dynamics. *Marine and Petroleum Geology*, 26(9), 1812-1823.
- 571 Flemings, P. B., Liu, X., and Winters, W. J., 2003, Critical pressure and multiphase flow in Blake Ridge
572 gas hydrates: *Geology*, v. 31, no. 12, p. 1057-1060.
- 573 Foucher, J.-P., Dupré, S., Scalabrin, C., Feseker, T., Harmegnies, F., and Nouzé, H., 2010, Changes in
574 seabed morphology, mud temperature and free gas venting at the Håkon Mosby mud volcano,
575 offshore northern Norway, over the time period 2003–2006: *Geo-Marine Letters*, v. 30, no. 3-4, p.
576 157-167.
- 577 Freudenthal, T., and Wefer, G., 2013, Drilling cores on the sea floor with the remote-controlled sea-floor
578 drilling rig MeBo: *Geosci. Instrum. Method. Data Syst. Discuss.*, v. 3, no. 2, p. 347-369.

- 579 Gay, A., Lopez, M., Cochonat, P., Levaché, D., Sermondadaz, G., and Seranne, M., 2006a, Evidences of
580 early to late fluid migration from an upper Miocene turbiditic channel revealed by 3D seismic
581 coupled to geochemical sampling within seafloor pockmarks, Lower Congo Basin: Marine and
582 Petroleum Geology, v. 23, no. 3, p. 387-399.
- 583 Gay, A., Lopez, M., Ondreas, H., Charlou, J. L., Sermondadaz, G., and Cochonat, P., 2006b, Seafloor
584 facies related to upward methane flux within a Giant Pockmark of the Lower Congo Basin: Marine
585 Geology, v. 226, no. 1–2, p. 81-95.
- 586 George, R. A., and Cauquil, E., AUV Ultrahigh-Resolution 3D Seismic Technique for Detailed Subsurface
587 Investigations, *in* Proceedings Offshore Technology Conference2007, Offshore Technology
588 Conference.
- 589 Ginsburg, G. D., Milkov, A. V., Soloviev, V. A., Egorov, A. V., Cherkashev, G. A., Vogt, P. R., Crane, K.,
590 Lorensen, T. D., and Khutorskoy, M. D., 1999, Gas hydrate accumulation at the Håkon Mosby
591 Mud Volcano: Geo-Marine Letters, v. 19, no. 1-2, p. 57-67.
- 592 Graue, K., 2000, Mud volcanoes in deepwater Nigeria: Marine and Petroleum Geology, v. 17, no. 8, p. 959-
593 974.
- 594 Greinert, J., Artemov, Y., Egorov, V., De Batist, M., and McGinnis, D., 2006, 1300-m-high rising bubbles
595 from mud volcanoes at 2080m in the Black Sea: Hydroacoustic characteristics and temporal
596 variability: Earth and Planetary Science Letters, v. 244, no. 1–2, p. 1-15.
- 597 Haeckel, M., Suess, E., Wallmann, K., and Rickert, D., 2004, Rising methane gas bubbles form massive
598 hydrate layers at the seafloor: Geochimica et Cosmochimica Acta, v. 68, no. 21, p. 4335-4345.
- 599 Hartwig, A., Anka, Z., and di Primio, R., 2012, Evidence of a widespread paleo-pockmarked field in the
600 Orange Basin: An indication of an early Eocene massive fluid escape event offshore South Africa:
601 Marine Geology, v. 332-334, p. 222-234.

- 602 Heggland, R., Vertical hydrocarbon migration at the Nigerian continental slope: applications of seismic
603 mapping techniques, *in* Proceedings AAPG Annual Meeting, Salt Lake City, May2003, p. 11-14.
- 604 Hoehler, T.M., Alperin, M.J., Albert, D.B., Martens, C.S., (1994) Field and laboratory studies of methane
605 oxidation in an anoxic marine sediment: Evidence for a methanogen-sulfate reducer consortium.
606 *Global Biogeochemical Cycles*, 8(4), 451-463.
- 607 Hovland, M., Gallagher, J. W., Clennell, M. B., and Lekvam, K., 1997, Gas hydrate and free gas volumes
608 in marine sediments: Example from the Niger Delta front: *Marine and Petroleum Geology*, v. 14,
609 no. 3, p. 245-255.
- 610 Judd, A. A. G., and Hovland, M., 2007, Seabed fluid flow: the impact of geology, biology and the marine
611 environment, Cambridge University Press.
- 612 Kopf, A. J., 2002, Significance of mud volcanism: *Reviews of Geophysics*, v. 40, no. 2, p. 1005.
- 613 Marcon, Y., Ondréas, H., Sahling, H., Bohrmann, G., and Olu, K., 2014, Fluid flow regimes and growth of
614 a giant pockmark: *Geology*, v. 42, no. 1, p. 63-66.
- 615 Masoudi, R., Tohidi, B., (2005) Estimating the hydrate stability zone in the presence of salts and/or organic
616 inhibitors using water partial pressure. *Journal of Petroleum Science and Engineering*, 46(1-2), 23-
617 36.
- 618 Matsumoto, R., Ryu, B.-J., Lee, S.-R., Lin, S., Wu, S., Sain, K., Pecher, I., and Riedel, M., 2011,
619 Occurrence and exploration of gas hydrate in the marginal seas and continental margin of the Asia
620 and Oceania region: *Marine and Petroleum Geology*, v. 28, no. 10, p. 1751-1767.
- 621 Moss, J. L., Cartwright, J., and Moore, R., 2012, Evidence for fluid migration following pockmark
622 formation: Examples from the Nile Deep Sea Fan: *Marine Geology*, v. 303-306, p. 1-13.

- 623 Pape, T., Feseker, T., Kasten, S., Fischer, D., Bohrmann, G., (2011) Distribution and abundance of gas
624 hydrates in near-surface deposits of the Håkon Mosby Mud Volcano, SW Barents Sea.
625 *Geochemistry, Geophysics, Geosystems*, 12(9), Q09009.
- 626 Pape, T., Geprägs, P., Hammerschmidt, S., Wintersteller, P., Wei, J., Fleischmann, T., Bohrmann, G., Kopf,
627 A.J., (2014) Hydrocarbon seepage and its sources at mud volcanoes of the Kumano forearc basin,
628 Nankai Trough subduction zone. *Geochemistry, Geophysics, Geosystems*, 15(6), 2180-2194.
- 629 Paull, C.K., Ussler III, W., Borowski, W.S., Spiess, F.N., (1995) Methane-rich plumes on the Carolina
630 continental rise: Associations with gas hydrates. *Geology*, 23(1), 89-92.
- 631 Paull, C. K., Ussler, W., Holbrook, W. S., Hill, T. M., Keaten, R., Mienert, J., Haflidason, H., Johnson, J.
632 E., Winters, W. J., and Lorenson, T. D., 2008, Origin of pockmarks and chimney structures on the
633 flanks of the Storegga Slide, offshore Norway: *Geo-Marine Letters*, v. 28, no. 1, p. 43-51.
- 634 Pilcher, R., and Argent, J., 2007, Mega-pockmarks and linear pockmark trains on the West African
635 continental margin: *Marine Geology*, v. 244, no. 1-4, p. 15-32.
- 636 Pinet, N., Duchesne, M., and Lavoie, D., 2010, Linking a linear pockmark train with a buried Palaeozoic
637 structure: a case study from the St. Lawrence Estuary: *Geo-Marine Letters*, v. 30, no. 5, p. 517-522.
- 638 Riboulot, V., Cattaneo, A., Sultan, N., Garziglia, S., Ker, S., Imbert, P., and Voisset, M., 2013, Sea-level
639 change and free gas occurrence influencing a submarine landslide and pockmark formation and
640 distribution in deepwater Nigeria: *Earth and Planetary Science Letters*, v. In Press, Corrected
641 Proof.
- 642 Riedel, M., Novosel, I., Spence, G. D., Hyndman, R. D., Chapman, R. N., Solem, R. C., and Lewis, T.,
643 2006, Geophysical and geochemical signatures associated with gas hydrate-related venting in the
644 northern Cascadia margin: *Geological Society of America Bulletin*, v. 118, no. 1-2, p. 23-38.

- 645 Rise, L., Sættem, J., Fanavoll, S., Thorsnes, T., Ottesen, D., and Bøe, R., 1999, Sea-bed pockmarks related
646 to fluid migration from Mesozoic bedrock strata in the Skagerrak offshore Norway: *Marine and*
647 *Petroleum Geology*, v. 16, no. 7, p. 619-631.
- 648 Ritger, S., Carson, B., Suess, E., (1987) Methane-derived authigenic carbonates formed by subduction-
649 induced pore-water expulsion along the Oregon/Washington margin. *Geological Society of*
650 *America Bulletin*, 98, 147-156.
- 651 Römer, M., Sahling, H., Pape, T., Bahr, A., Feseker, T., Wintersteller, P., and Bohrmann, G., 2012,
652 Geological control and magnitude of methane ebullition from a high-flux seep area in the Black
653 Sea—the Kerch seep area: *Marine Geology*, v. 319–322, no. 0, p. 57-74.
- 654 Sahling, H., Bohrmann, G., Spiess, V., Bialas, J., Breitzke, M., Ivanov, M., Kasten, S., Krastel, S., and
655 Schneider, R., 2008, Pockmarks in the Northern Congo Fan area, SW Africa: Complex seafloor
656 features shaped by fluid flow: *Marine Geology*, v. 249, no. 3-4, p. 206-225.
- 657 Seeberg-Elverfeldt, J., Schlüter, M., Feseker, T., Kölling, M., (2005) Rhizon sampling of porewaters near
658 the sediment-water interface of aquatic systems. *Limnology and Oceanography: Methods*, 3, 361-
659 371.
- 660 Sloan, E. D., and Koh, C., 2007, *Clathrate hydrates of natural gases*, CRC press.
- 661 Sultan, N., Bohrmann, G., Ruffine, L., Pape, T., Riboulot, V., Colliat, J. L., De Prunelé, A., Dennielou, B.,
662 Garziglia, S., Himmler, T., Marsset, T., Peters, C. A., Rabiou, A., and Wei, J., 2014, Pockmark
663 formation and evolution in deep water Nigeria: Rapid hydrate growth versus slow hydrate
664 dissolution: *Journal of Geophysical Research: Solid Earth*, v. 119, no. 4, p. 2013JB010546.
- 665 Sultan, N., Marsset, B., Ker, S., Marsset, T., Voisset, M., Vernant, A.-M., Bayon, G., Cauquil, E., Adamy,
666 J., and Colliat, J., 2010, Hydrate dissolution as a potential mechanism for pockmark formation in
667 the Niger delta: *Journal of geophysical research*, v. 115, no. B8, p. B08101.

- 668 Sun, Q., Wu, S., Hovland, M., Luo, P., Lu, Y., and Qu, T., 2011, The morphologies and genesis of mega-
669 pockmarks near the Xisha Uplift, South China Sea: *Marine and Petroleum Geology*, v. 28, no. 6, p.
670 1146-1156.
- 671 Torres, M. E., Kim, J.-H., Choi, J.-Y., Ryu, B.-J., Bahk, J.-J., Riedel, M., Collett, T. S., Hong, W.-L., and
672 Kastner, M., Occurrence of high salinity fluids associated with massive near-seafloor gas hydrate
673 deposits, *in Proceedings 7th International Conference on Gas Hydrates (ICGH 2011)*2011.
- 674 Torres, M. E., Teichert, B. M. A., Tréhu, A. M., Borowski, W., and Tomaru, H., 2004a, Relationship of
675 pore water freshening to accretionary processes in the Cascadia margin: Fluid sources and gas
676 hydrate abundance: *Geophysical Research Letters*, v. 31, no. 22, p. L22305.
- 677 Torres, M. E., Wallmann, K., Tréhu, A. M., Bohrmann, G., Borowski, W. S., and Tomaru, H., 2004b, Gas
678 hydrate growth, methane transport, and chloride enrichment at the southern summit of Hydrate
679 Ridge, Cascadia margin off Oregon: *Earth and Planetary Science Letters*, v. 226, no. 1-2, p. 225-
680 241.
- 681 Tréhu, A. M., Long, P. E., Torres, M. E., Bohrmann, G., Rack, F. R., Collett, T. S., Goldberg, D. S.,
682 Milkov, A. V., Riedel, M., Schultheiss, P., Bangs, N. L., Barr, S. R., Borowski, W. S., Claypool, G.
683 E., Delwiche, M. E., Dickens, G. R., Gracia, E., Guerin, G., Holland, M., Johnson, J. E., Lee, Y. J.,
684 Liu, C. S., Su, X., Teichert, B., Tomaru, H., Vanneste, M., Watanabe, M., and Weinberger, J. L.,
685 2004, Three-dimensional distribution of gas hydrate beneath southern Hydrate Ridge: constraints
686 from ODP Leg 204: *Earth and Planetary Science Letters*, v. 222, no. 3-4, p. 845-862.
- 687 Ussler III, W., Paull, C.K., (1995) Effects of ion exclusion and isotopic fractionation on pore water
688 geochemistry during gas hydrate formation and decomposition. *Geo-Marine Letters*, 15(1), 37-44.
- 689 Ussler, W., III, Paull, C. K., Boucher, J., Friederich, G. E., and Thomas, D. J., 2003, Submarine pockmarks:
690 a case study from Belfast Bay, Maine: *Marine Geology*, v. 202, no. 3-4, p. 175-192.

- 691 Waite, W. F., Stern, L. A., Kirby, S. H., Winters, W. J., and Mason, D. H., 2007, Simultaneous
692 determination of thermal conductivity, thermal diffusivity and specific heat in sI methane hydrate:
693 *Geophysical Journal International*, v. 169, no. 2, p. 767-774.
- 694 Wallmann, K., Aloisi, G., Haeckel, M., Obzhairov, A., Pavlova, G., and Tishchenko, P., 2006, Kinetics of
695 organic matter degradation, microbial methane generation, and gas hydrate formation in anoxic
696 marine sediments: *Geochimica et Cosmochimica Acta*, v. 70, no. 15, p. 3905-3927.
- 697 Weinberger, J. L., Brown, K. M., and Long, P. E., 2005, Painting a picture of gas hydrate distribution with
698 thermal images: *Geophysical Research Letters*, v. 32, no. 4, p. L04609.
- 699
- 700

701

702 **Figure captions:**

703 Figure 1: (A): Location of the pockmark field at the Nigerian continental margin. (B): Overview
704 of the studied pockmark field. (C) and (D): MeBo drill sites (GMMB) in pockmarks A and C (C1
705 and C2), respectively. Numbers refer to individual MeBo station codes (i.e. No. 01 = station
706 GMMB01, for example) Track lines of SYSIF seismic profiles SY03-THR-Pr01 and SY01-HR-
707 Pr02 as well as the shot points are shown. For exact positions refer to Sultan et al. (2014).

708 Figure 2: Combined illustration of core photographs (left) and IR images (right) of the 6.6 m-long
709 MeBo drill core GMMB06. Representative intervals of the core (A, B and C) are shown in detail
710 (right part of the figure). (A): normal hemi-pelagic sediment (upper part) and voids (lower part),
711 which in the IR images correspond to the background temperature (orange) and high temperature
712 (yellow), respectively. The bright spot (white) is an artifact generated during the core handling.
713 (B): Moussy sediment with cracks, which in the IR image shows three cold temperature zones
714 (light purple) caused by the dissociation of disseminated gas hydrates. (C): Soupy and fluidized
715 sediments. The cold temperature interval below 5.70 mbsf contained gas hydrates including a
716 nodular gas hydrate between 5.80 and 5.85 mbsf represented by an extremely cold spot (dark
717 purple to black). GH = gas hydrate

718 Figure 3: IR temperatures and pore water chloride concentration profiles of MeBo cores. Four
719 data sets are shown for most drill sites: IR image colors, IR temperature profiles, interpreted gas
720 hydrate distributions, and chloride profiles. The color bar of the IR images is consistent with Fig.
721 2 and white intervals indicate gaps. Temperature profiles show the differences between the
722 measured temperature and background temperatures of core liners, expressed as ΔT . Positive ΔT
723 values correlate with voids in the cores and negative ΔT values represent decomposing gas
724 hydrates. The approximate down-core gas hydrate presence interpreted from IR images is

725 indicated by colored bars and indications for depth below seafloor (mbsf). Depths of gas hydrate-
726 bearing intervals as inferred from chloride anomalies are highlighted in blue shading. Note that
727 the chloride data of the upper 12.7 mbsf at station GMMB09 were derived from a piston core
728 (GMCS10) taken at the same position.

729 Figure 4: A: Position of sites chosen for temperature measurements in pockmark A. B: *In situ*
730 sediment temperature measurements. Temperature gradients were classified into two clusters: (1)
731 background gradients (around 72 °C/km) highlighted by the dark grey background, and (2) high
732 gradients caused by fluid advection without background color.

733 Figure 5: Temperature change with time at stations GMGCT40 and GMGCT41. TL-1 to TL-5
734 represents the temperature sensors attached to the corer from base to top. Remarkably, the
735 temperature measured with TL-2 at station GMGCT40 increased continuously after penetration
736 and was higher than that of TL-1, which penetrated deeper into the sediment. Note that TL-5 had
737 no contact with sediment and, therefore, measured bottom water temperature.

738 Figure 6: Phase diagram calculated for structure I gas hydrates with the HWHYD software
739 (Masoudi and Tohidi, 2005) and using salinities and pure methane because methane concentration
740 of hydrate-bounded gas is higher than 99.9% (unpublished data). A CTD record was used to show
741 the water column temperature profile. 72 °C/km (GMGCT22) was used as the local background
742 geothermal gradient outside the pockmarks, while 258 °C/km (GMGCT45) was measured close
743 to a site at pockmark center which showed seafloor gas emission (see Sultan et al., 2014). The
744 subsurface part (dash blue rectangle) of the diagram is enlarged in the right part of the figure.

745 Figure 7: SYSIF seismic profiles SY03-THR-Pr01 crossing pockmark A and SY01-THR-Pr02
746 covering pockmark cluster C. Locations and orientations are shown in Fig. 1. Interpretations from
747 MeBo cores are projected on the seismic lines. High-amplitude reflectors are widespread in the
748 seismic profile.

749 Figure 8: Schematic representations of the pockmark formation controlled by fluid flow and gas
750 hydrate precipitation during different evolutionary stages (A-E).

751

ACCEPTED MANUSCRIPT

1

2 Table 1: Basic information of the MeBo cores taken during the Guenco-MeBo cruise as well as
 3 upper and lower boundaries of the gas hydrate occurrence zone (GHOZ) estimated using IR
 4 thermal scanning and pore water chloride concentration anomalies, respectively. mbsl: meters
 5 below sea level. mbsf: meters below seafloor. nd: not detected. nc: not calculated.

6

Sample code	Location	Water depths (mbsl)	Core length (m)	Top and base of gas hydrate occurrence in cores (mbsf)			
				Deduced from IR thermal scanning		Deduced from chloride profiling	
				Top	Base	Top	Base
				GMMB01&02	NW of pockmark A	1141	53.30
GMMB03	Pockmark A	1148	45.18	6.9	17.6	6.15-6.95	18.09-22.00
GMMB06	Pockmark A	1148	6.67	3.1	6.6	2.05-3.40	6.67
GMMB07	Pockmark A	1148	10.19	5.0	10.2	1.40-2.85	10.19
GMMB08	Pockmark A	1142	56.74	2.3	26.2	1.44-5.35	22.69-24.14
GMMB10	Pockmark A	1145	23.95	nc.	nc.	4.45-5.15	23.95
GMMB11	Pockmark A	1146	12.58	6.5	12.5	1.20-6.65	12.58
GMMB12	Pockmark A	1144	24.57	7.6	17.1	6.76-7.26	17.94-18.44
GMMB04	Pockmark C1	1189	18.61	5.9	18.5	5.28-6.08	18.61
GMMB05	Pockmark C2	1199	52.36	10.3	13.0	8.50-10.65	19.05-19.64
GMMB09	SE of Pockmark C2	1196	43.64	38.5	43.6	38.46-38.83	43.64

7

8

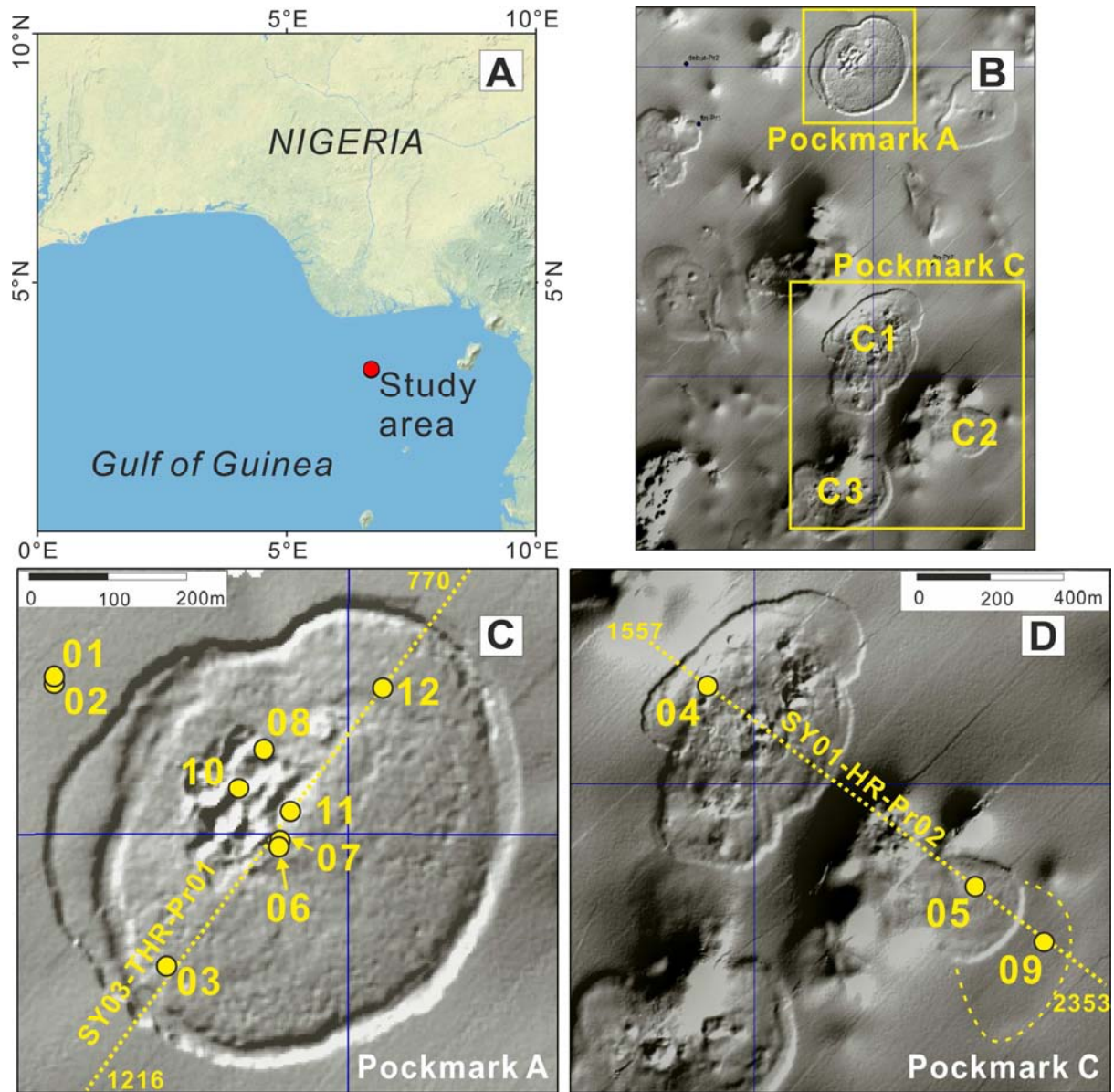
1

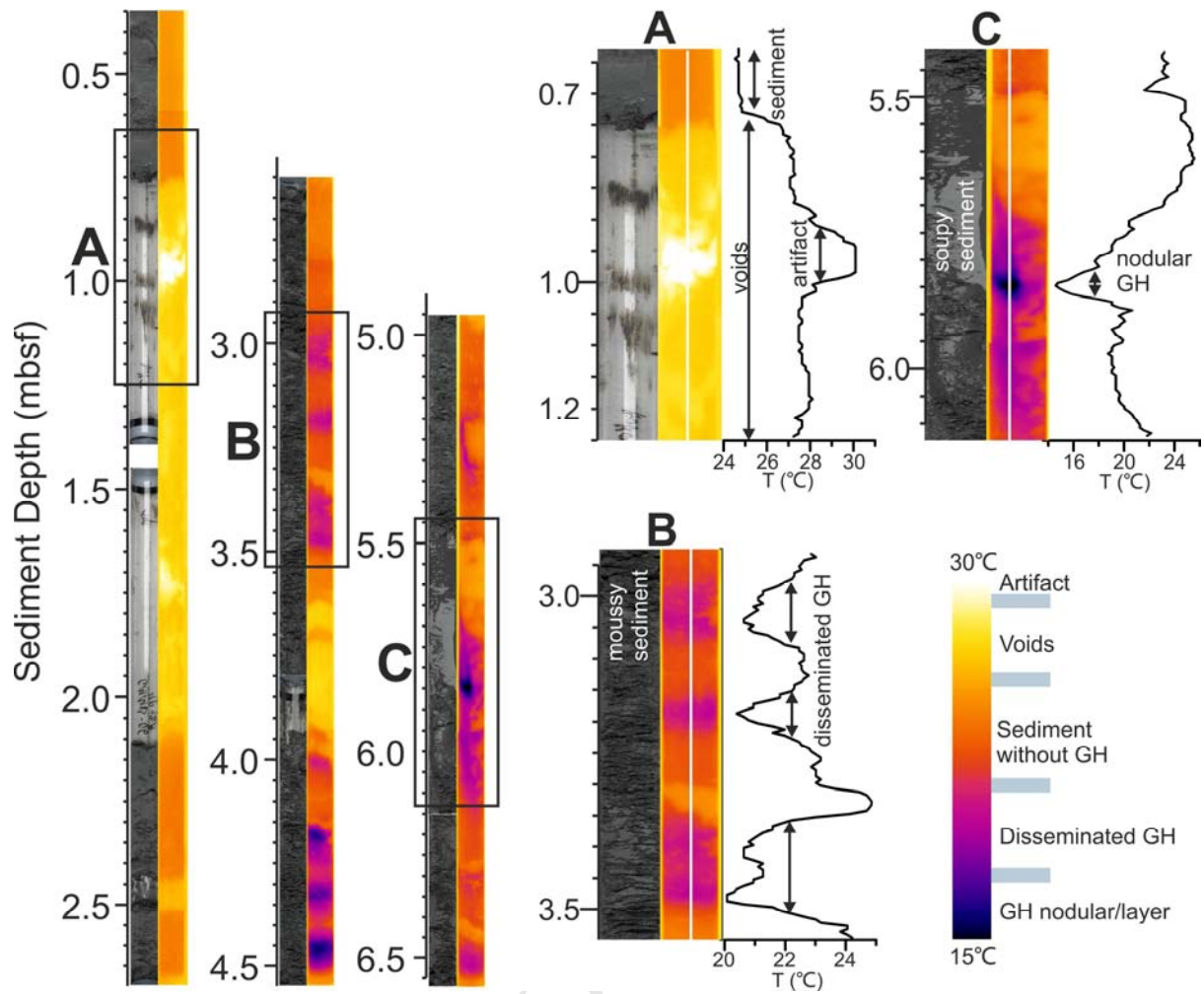
2 Table 2: Stations of *in situ* sediment temperature measurements in pockmark A with temperatures
 3 probes (GMGCT) during the Guineco-MeBo cruise. For calculation of STD, water temperatures
 4 measured 50 m above seafloor with the MTLs at individual stations were used. *Note: because of
 5 the non-linear slope of the profile this gradient was not considered further

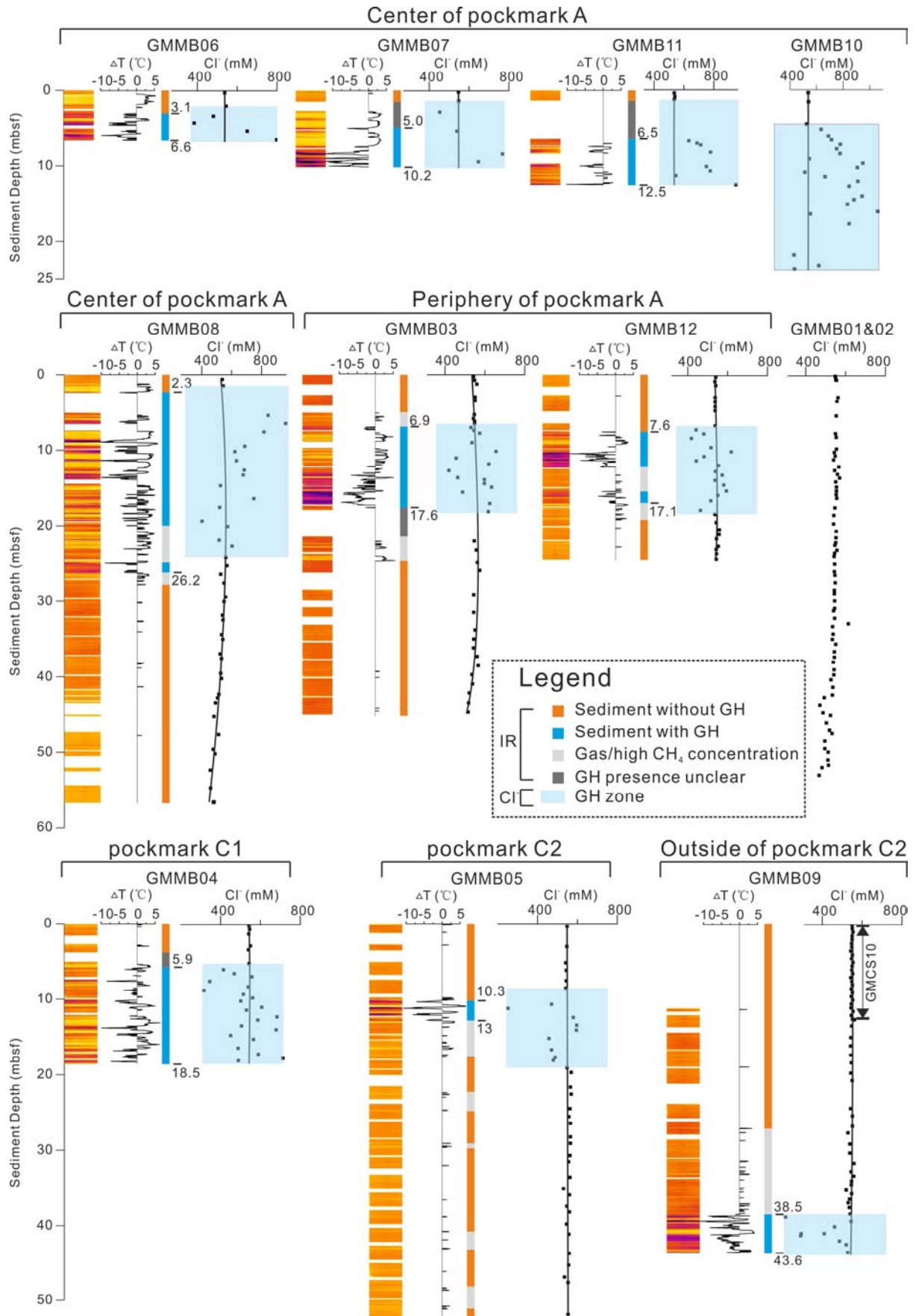
6 n: number of probes from which geothermal gradients were calculated.

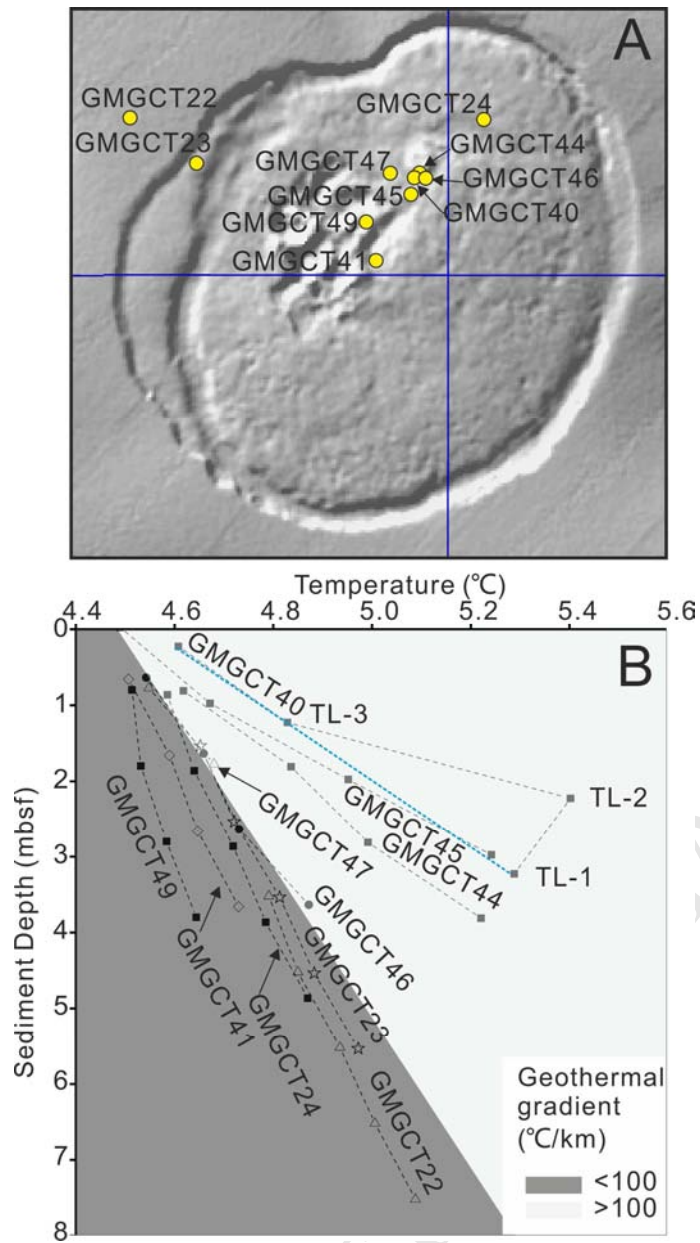
	Water depth (m)	Water temperature (°C)	STD (°C)	Thermal gradients (°C/km)	n
GMGCT22	1144	4.53	0.006	72	5
GMGCT23	1142	4.52	0.005	79	5
GMGCT24	1143	4.52	0.005	70	5
GMGCT40	1144	4.46	0.005	330*	4
GMGCT41	1143	4.46	0.005	73	4
GMGCT44	1140	4.46	0.005	198	4
GMGCT45	1141	4.45	0.004	258	4
GMGCT46	1140	4.46	0.008	112	4
GMGCT47	1141	4.46	0.006	119	2
GMGCT49	1142	4.45	0.007	51	4

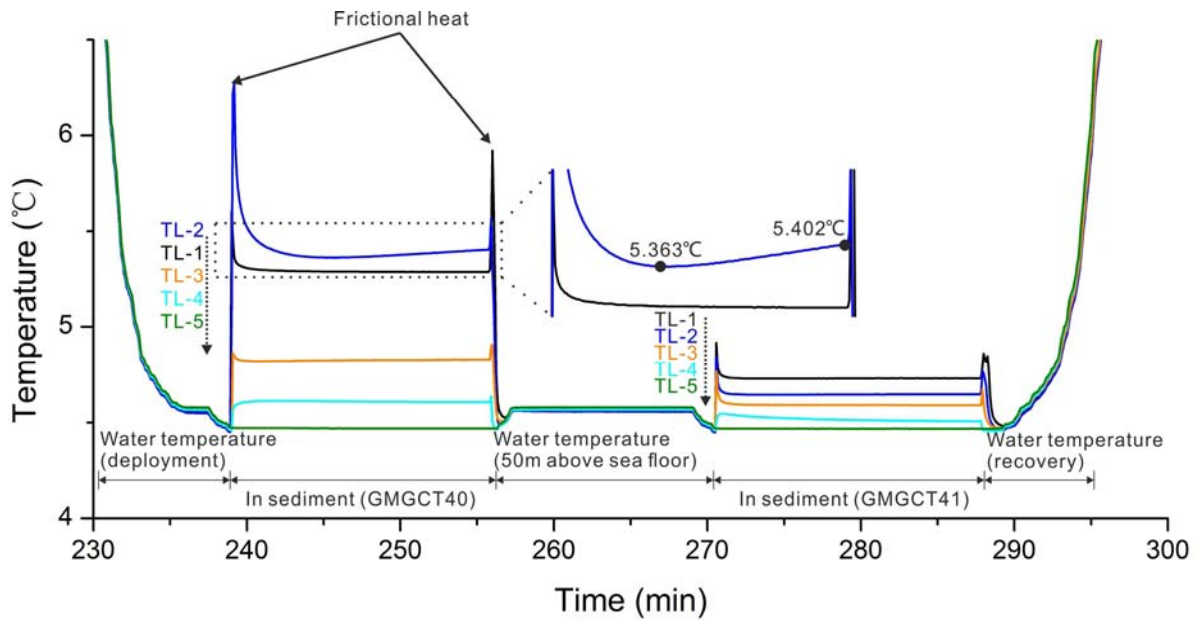
7

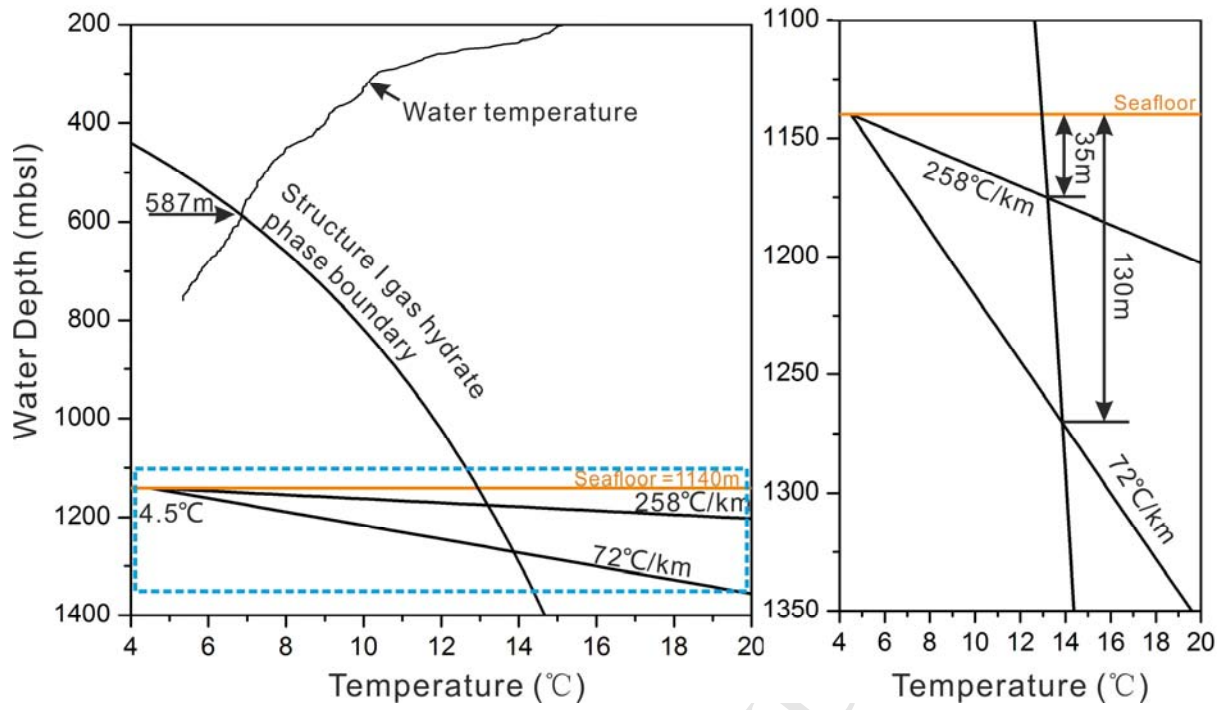


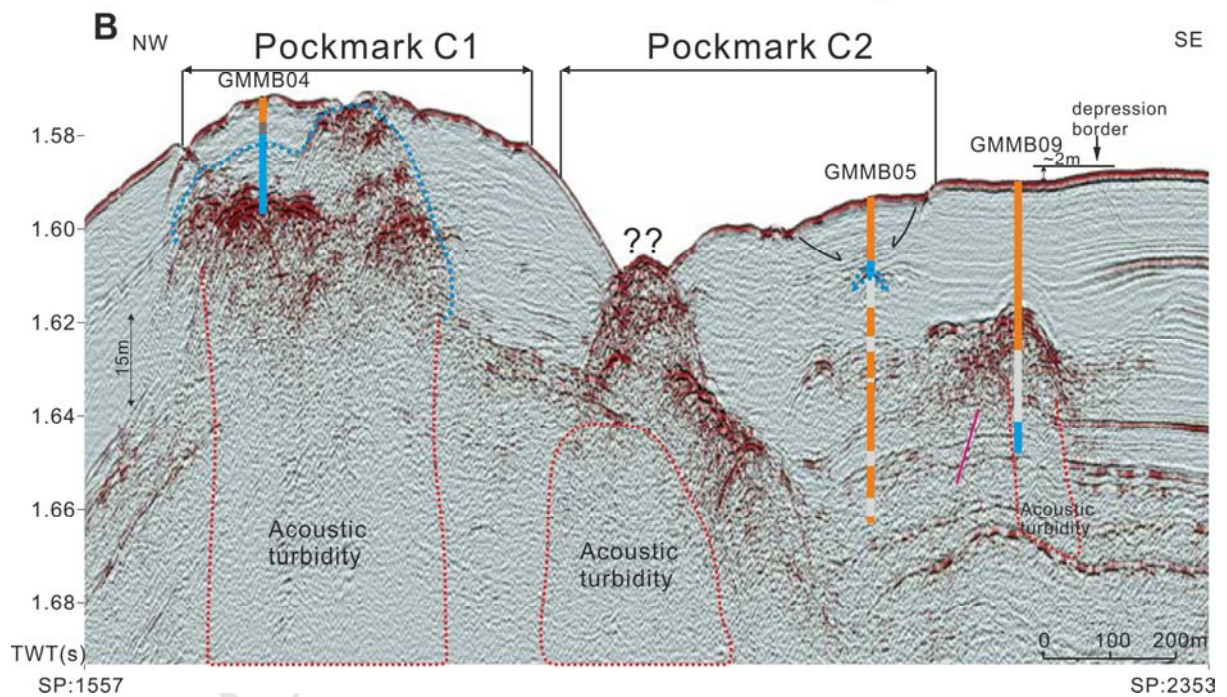
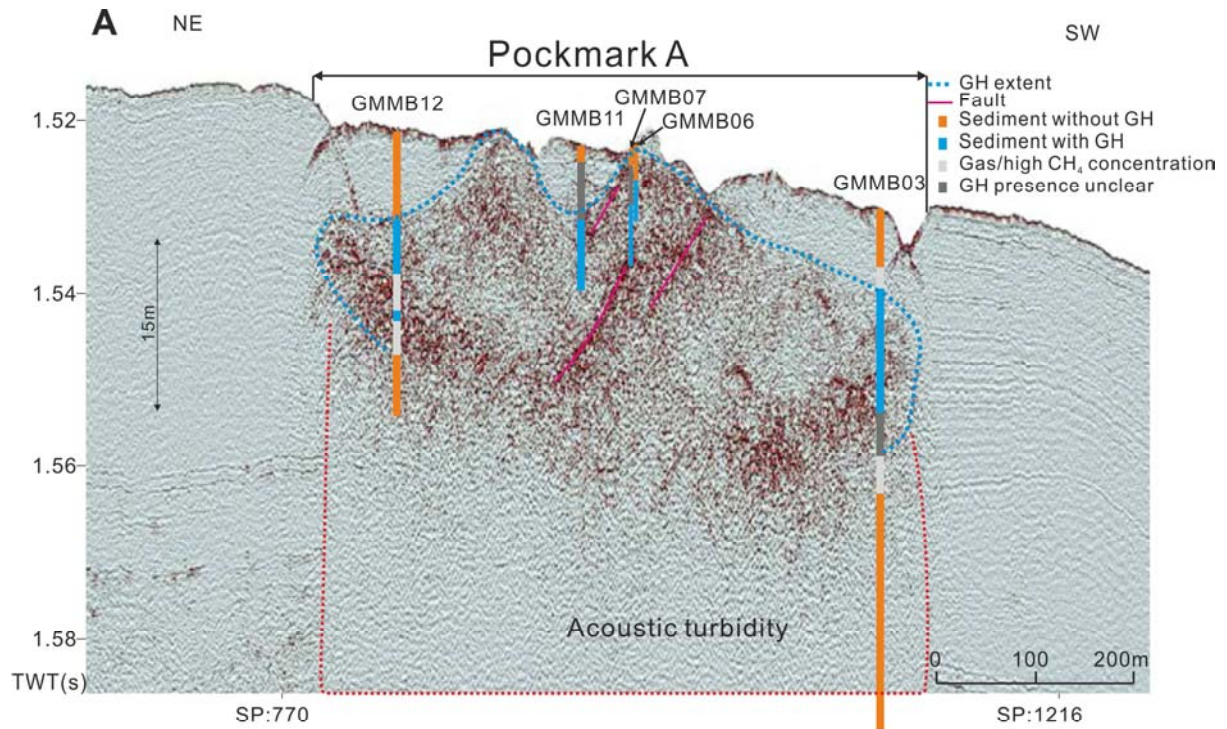


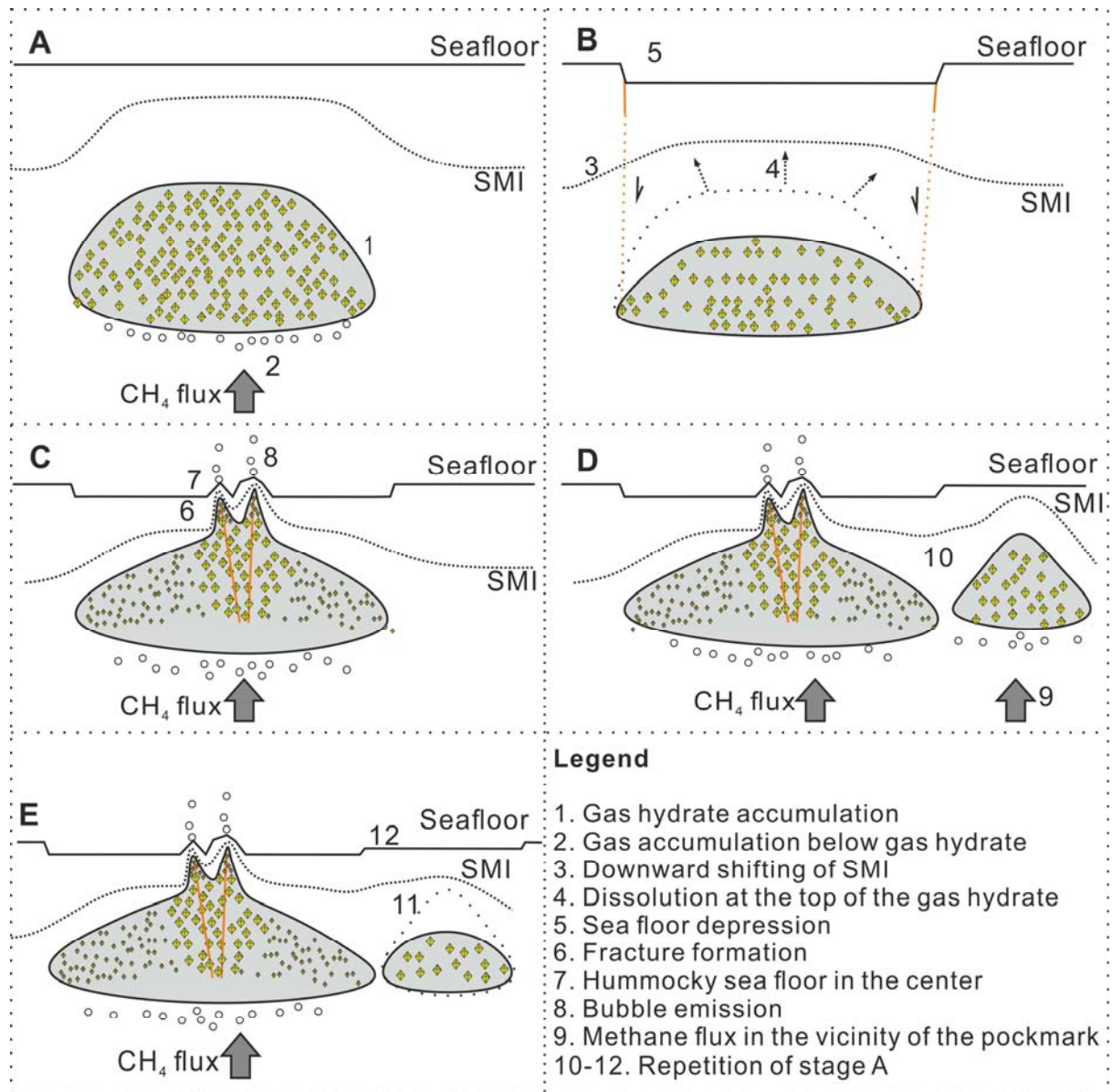












Highlights:

1. Pockmarks on the Nigerian continental margin were investigated for gas hydrates
2. Long sediment cores were recovered with the portable MeBo drill rig
3. Infrared and pore water chloride measurements revealed gas hydrate distributions
4. Geothermal gradients in the pockmark center up to five fold higher than at the rim
5. Fluid flow and gas hydrate dynamics influence the evolution of pockmarks